Robust nature of the chiral spin helix in $CrNb_3S_6$ nanostructures studied by off-axis electron holography

Dongsheng Song[1], Lin Wang[2], Weiwei Wang[3], Fengshan Zheng[1], Jin Tang[4], Shasha Wang[4], Chao Zhu[5], Jan Caron[1], András Kovács[1], Zheng Liu[5], David Mandrus[6,7,8], Mingliang Tian[4], Haifeng Du[3,4,9*], Rafal E. Dunin-Borkowski[1]

[1] Ernst Ruska-Centre for Microscopy and Spectroscopy with Electrons and Peter Grünberg Institute, Forschungszentrum Jülich, 52425 Jülich, Germany

[2] Key Laboratory of Flexible Electronics (KLOFE) & Institute of Advanced Materials (IAM), Jiangsu National Synergetic Innovation Center for Advanced Materials (SICAM), Nanjing Tech University (NanjingTech), 30 South Puzhu Road, Nanjing 211816, China

[3] Institutes of Physical Science and Information Technology, Anhui University, Hefei, 230601, China

[4] Anhui Province Key Laboratory of Condensed Matter Physics at Extreme Conditions, High Magnetic Field Laboratory, Chinese Academy of Sciences and University of Science and Technology of China, Hefei 230026, China

[5] School of Materials Science and Engineering, Nanyang Technological University, Singapore 639798, Singapore.

[6] Department of Materials Science and Engineering, University of Tennessee, Knoxville, Tennessee 37996, USA

[7] Theoretical Division, T-4 and CNLS, Los Alamos National Laboratory, Los Alamos, New Mexico 87545, USA

[8] Department of Physics and Astronomy, University of Tennessee, Knoxville, Tennessee 37996, USA

[9] Collaborative Innovation Center of Advanced Microstructures, Nanjing University, Jiangsu Province 210093, China

E-mail: duhf@hmfl.ac.cn

Dongsheng Song and Lin Wang contributed equally.

Abstract

Magnetic soliton crystals with layered structures that host periodic chiral helimagnetic ordering are the promising candidates for spintronic nanodevices. Among them, helimagnetic $CrNb_3S_6$ is unique owing to its crystallographic chirality and monoaxial Dzyaloshinskii-Moriya interaction (DMI). It is crucial to explore the magnetic configurations and properties with respect to the temperature and thickness especially in reduced dimensions. Here, the chiral helimagnetic ground state in $CrNb_3S_6$ nanostructures is investigated using off-axis electron holography in the transmission electron microscope. The period of the helical state is found to be independent of both temperature and specimen thickness, while the temperature dependence of the saturation magnetization is shown to follow a classical Heisenberg spin model. Monte Carlo simulations based on a discrete classical Heisenberg model reproduce the experimental observations closely, confirming the applicability of a three-dimensional Heisenberg model even in a confined specimen geometry.

Chirality is common in nature, for instance in crystallography, where the absence of mirror symmetry in atomic configurations can be decisive for material properties. In magnetic materials, crystal symmetry can give rise to chiral interactions, such as the Dzyaloshinskii-Moriya interaction (DMI), which can be the source of multiferroic behavior [1,2] and can result in the formation of exotic magnetic objects such as skyrmions [3,4], chiral bobbers [5] and solitons [6]. DMI-hosting magnetic materials include B20-type FeGe, MnSi and Cu_2OSeO_3, β-Mn-type CoZnMn and $Fe_xCo_{1-x}Rh_{0.5}Mo_3N$ and hexagonal $CrNb_3S_6$ [1]. $CrNb_3S_6$ is a monoaxial helimagnet [7,8] as one of the promising candidates of magnetic two-dimensional crystals, in which competition between DMI and exchange coupling can lead to periodic chiral helimagnetic (CHM) order in the form of sinusoidal stripe domains [6–10]. If an external magnetic field is applied perpendicular to the helical axis of $CrNb_3S_6$, then a chiral magnetic soliton lattice (CSL) rather than a skyrmion lattice can form as a result of the uniaxial nature of the DMI [6]. Magneto-transport measurements have shown that conduction electrons can couple with CSLs, resulting in unique interlayer magnetoresistance [11] and electrical magneto-chiral [12] effects. In magnetic nanostructures that have confined geometries, $CrNb_3S_6$ exhibits discretized magnetoresistance or magnetization jumps as a result of confinement of the CSL [13,14], motivating the need to understand the magnetic behavior of CHM order and CSLs in $CrNb_3S_6$ nanostructures on the nanoscale. Although Lorentz transmission electron microscopy (LTEM) has been used to image CHM order and CSLs [6,13,15–17] in thin plates of $CrNb_3S_6$, quantitative studies of their magnetization in nanostructures are still lacking.

Here, we use off-axis electron holography (EH) to measure the projected in-plane magnetic moment distributions in $CrNb_3S_6$ nanostructures [18], in order to investigate the period and magnetization of CHM order as a function of temperature and specimen thickness. We use Monte Carlo (MC) simulations that include DMI and ferromagnetic exchange interactions to validate our experimental findings. Significantly, we find that the period of CHM order is independent of both temperature and specimen thickness. We measure a saturation magnetization-temperature (M_S-T) curve using off-axis EH and find it to be similar to that predicted using a classical Heisenberg model. Our results demonstrate the robust magnetic character of CHM order in geometrically-confined $CrNb_3S_6$ nanostructures.

Single crystalline $CrNb_3S_6$ was synthesized using a chemical vapor transport method. Two $CrNb_3S_6$ nanostructures with desired geometries were prepared for TEM experiments using a top-down focused ion beam (FIB) milling method. One of the nanostructures took the form of a thin plate with a uniform thickness of approximately 100 nm, while the other took the form of a wedge-shaped nanostripe with a continuously varying thickness of between 70 and 240 nm, as shown schematically in Figure S1 in the Supplemental Material [19]. Off-axis EH experiments were performed in magnetic-field-free conditions in Lorentz mode using an image spherical

aberration corrected FEI Titan 60-300 TEM operated at 300 kV. A liquid-N_2-cooled TEM specimen holder (Gatan 636) was used to control the specimen temperature between 95 and 380 K. Off-axis electron holograms were recorded using a single electrostatic biprism and a direct electron counting camera (Gatan K2-IS) with an interference fringe spacing of 2.78 nm and a fringe contrast of more than 65% [20]. Each experiment involved the acquisition of 25 object holograms, followed by 25 vacuum reference holograms to remove image distortions associated with the imaging and recording system of the microscope. Averaging of the holograms, which were each acquired using an exposure time of 4 s, was used to improve the signal-to-noise ratio. Phase images were reconstructed using a standard Fourier-transform-based approach in Holoworks 6.0 software (Holowork LLC) [21]. The mean inner potential (MIP) contribution to the phase was removed by taking the difference between phase images that had been recorded below the Curie temperature and at room temperature. The procedure that was used to retrieve experimental magnetic phase images is summarized in Figure S2 in the Supplemental Material [19].

$CrNb_3S_6$ has a hexagonal layered structure with alternating Cr and NbS_2 planes along the *c* axis, as shown in Figure 1(a). The Cr atoms are ferromagnetically coupled in the *ab* plane, while CHM order forms in the *c* direction as a result of a monoaxial DM interaction. Figure 1(b) shows the CHM spin texture in $CrNb_3S_6$, which has a period of $L = 48$ nm and is determined by the relative strength of the DMI constant D and the ferromagnetic exchange interaction constant J [6,13,15]. TEM samples were prepared with the *c* axis aligned in the sample plane and perpendicular to the incident electron beam direction (*z* axis), as marked by a red arrow in Figure 1(b). The projected in-plane magnetization shown in Figure 1(b) exhibits a sinusoidal variation along the *c* axis. It should be noted that only the magnetic field perpendicular to the electron beam direction contributes to the magnetic phase shift φ_M recorded using off-axis EH [18]. φ_M is defined as $-e/\hbar \int A_z \mathrm{d}z$, where A_z is the z component of the magnetic vector potential and e and $\hbar$ are the electron charge and the reduced Planck constant, respectively. If demagnetizing fields can be neglected, then for standard CHM order with $\boldsymbol{m}(x,y,z) = (0, \cos(2\pi x/L), \sin(2\pi x/L))$ in a specimen of uniform thickness t, the magnetic phase shift is defined as $\varphi_M = -\mu_0 M_s L t/2\Phi_0 \cdot \cos(2\pi x/L)$, where $\boldsymbol{m}$ is the magnetization, μ_0 is the vacuum permeability, Φ_0 is the magnetic flux quantum, M_S is the saturated magnetization and the *x* axis is parallel to the crystallographic *c* axis. Figure 1(c) shows a typical calculated magnetic phase shift image in the form of sinusoidal stripe pattern with a period of 48 nm, assuming a $CrNb_3S_6$ nanoplate thickness of 100 nm and a magnetic moment of 1.9 μ_B per Cr atom at 95 K. The magnetic phase shift can be used to obtain a magnetic induction map by adding contours and colors that represent the strength and direction of the projected in-plane magnetic induction. Figure 1(d) shows the resulting one-dimensional characteristic of the CHM order, with zero *x* component of the projected in-plane magnetic induction.

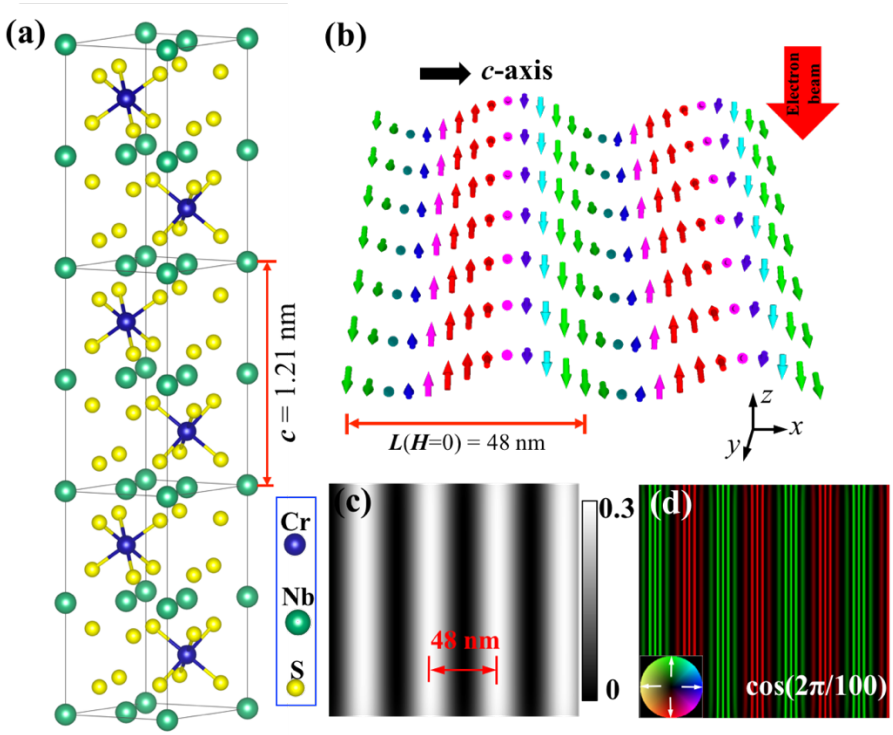

Figure 1. Measurement of magnetic structures in $CrNb_3S_6$ using off-axis electron holography. (a) Crystal structure of $CrNb_3S_6$, with the helix along the *c* axis. (b) Schematic diagram of a chiral helimagnetic structure with a period of 48 nm along the *c* axis in zero magnetic field. The electron beam direction is along the *z* axis. (c) Magnetic phase shift image of $CrNb_3S_6$ calculated for a nanoplate with a thickness of 100 nm and a magnetic moment of 1.9 μ_B per Cr atom at 95 K based on standard chiral helimagnetic order. (d) Magnetic induction map calculated from the gradient of the magnetic phase image shown in (c). The phase contour spacing is $2\pi/100 = 0.0628$ radians. The green and red colors indicate that the projected in-plane magnetic induction is oriented upwards and downwards, respectively.

Figure 2(a) shows experimental magnetic phase images recorded at four different temperatures between 95 and 133 K in a nanoplate of $CrNb_3S_6$ that has a uniform thickness of approximately 100 nm, similar to that shown in Figure 1(c). The CHM order can be seen to persist with increasing temperature. The line intensity profiles of φ_M shown in Figure 2(b) were extracted from the corresponding magnetic phase images shown in Figure 2(a). The decrease in the magnitude of φ_M suggests that the magnetization in the nanoplate decreases with increasing temperature. At 133 K, the variations in φ_M approach zero, corresponding to the CHM-paramagnetic phase transition. The magnetic induction contours shown in Figure 2(c) are then more widely separated. They are completely absent when the temperature of the specimen reaches 133 K.

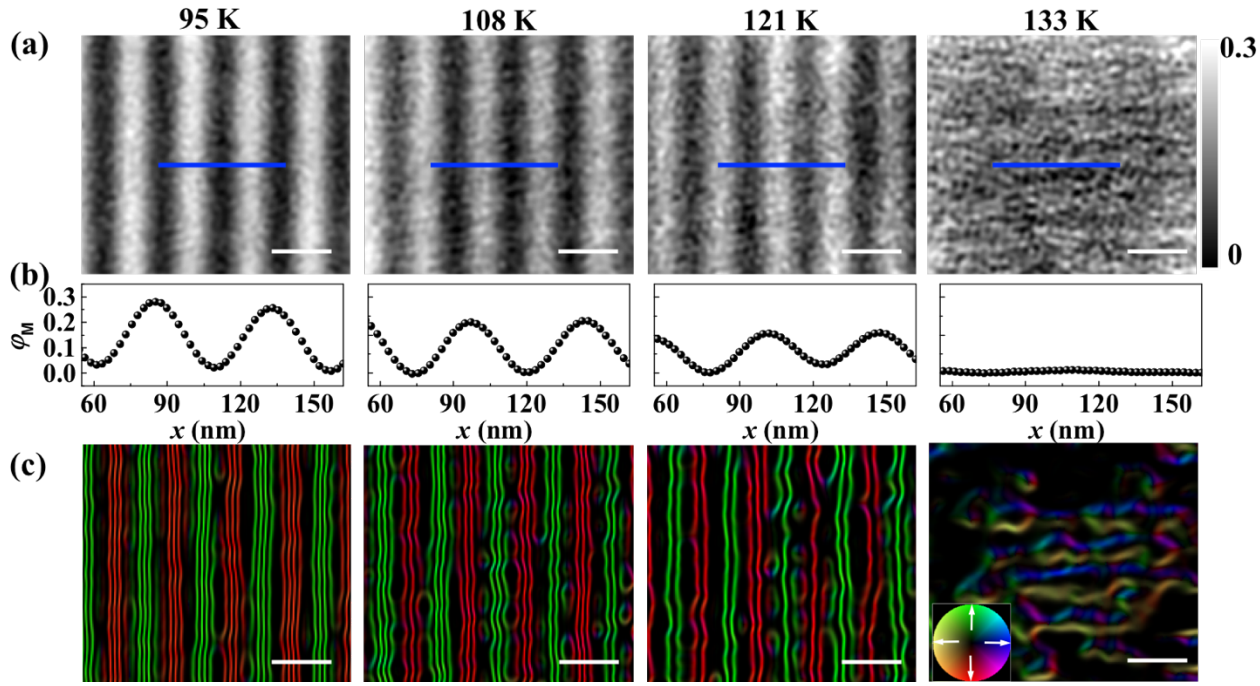

Figure 2. Chiral helimagnetic structure in a $CrNb_3S_6$ nanoplate measured as a function of temperature in zero magnetic field. (a) Magnetic phase shift images recorded at four different specimen temperatures using off-axis electron holography. The white and black levels correspond to the magnitude of the phase shift φ_M. (b) Line profiles of φ_M extracted along the blue lines marked in (a). (c) Magnetic induction maps of CHM order determined from the experimental magnetic phase images shown in (a). The phase contour spacing is $2\pi/100 = 0.0628$ radians. At 133 K, no measurable magnetic signal is present. All of the scale bars are 50 nm.

Quantitative real space maps of the projected in-plane magnetization $\boldsymbol{m}_{xy}$ were retrieved from the experimental magnetic phase shift images using a model-based iterative reconstruction algorithm [22]. Figure 3(a) shows the *y* component of the projected in-plane magnetization (normalized to μ_B per Cr atom) calculated from the experimental phase images recorded at different specimen temperatures. The *x* component of the projected in-plane magnetization is negligible, as shown in Figure S3 in the Supplemental Material [19]. The magnetization profiles at different temperatures shown in Figure 3(b) are consistent with the sinusoidal spin model of CHM shown in Figure 1(b). The magnetic moment per Cr atom can be inferred to be approximately 1.9 μ_B at 95 K, in agreement with previous experimental macro-measurement results [8]. The saturated magnetization (M_S) was determined by averaging the peak values in each magnetic stripe shown in Figure 3(b). The M_S-T curve, which is shown in Figure 3(c), exhibits a monotonic decrease in M_S with increasing temperature, as it approaches the Curie temperature. By fitting the measured M_S-T curve to a function of the form $M(T) = (1 - T/T_c)^{\beta}$, values of $\beta = 0.34$ and a Curie temperature of $T_c = 130$ K were obtained. The fitted value for T_c is consistent with that expected for a bulk crystal

(130 ± 2 K) in literatures [7,8] as well as our macro measurement (130.4 K) in Figure S4 in the Supplemental Material [19]. The phase transition from chiral incommensurate state to paramagnetic state occurs at T_c owing to the thermal fluctuations. These observations show that a thin nanoplate has similar magnetic properties to those in a bulk crystal and exhibits high stability of CHM order in a dimensionally-confined $CrNb_3S_6$ system.

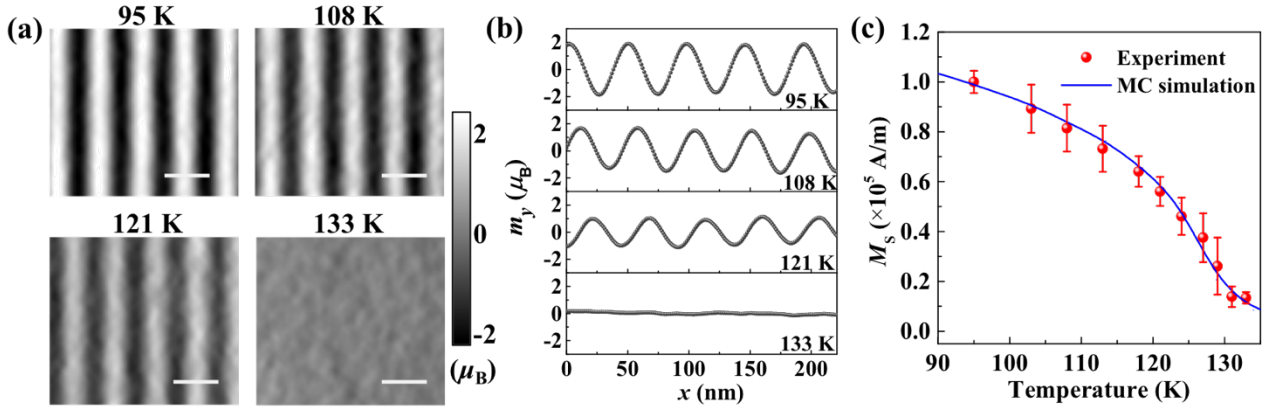

Figure 3 Quantitative measurements of magnetization in a $CrNb_3S_6$ nanoplate. (a) Reconstructed real space distributions of the y component of the projected in-plane magnetization (normalized to μ_B per Cr atom) measured at the indicated temperatures using a model-based iterative reconstruction algorithm. The white and black levels correspond to the magnitude of the projected in-plane magnetization. The scale bars are 50 nm. (b) Line profiles of the y component of the projected in-plane magnetization extracted from the images shown in (a) for the indicated temperatures. (c) Saturation magnetization (M_S) plotted as a function of temperature between 95 and 135 K. The Curie temperature is measured to be 130 K. Experimental data are plotted using red circles, while the results of Monte Carlo (MC) simulations are plotted in blue.

Monte Carlo (MC) simulations were performed to interpret the experimental results using a classical Heisenberg model for a monoaxial chiral magnet. Models for equilibrium helical states at different temperatures were obtained using a MC method based on a discrete Hamilton, which contains terms describing Heisenberg ferromagnetic exchange, DMI and magnetic anisotropy. The parameters J_{ab} = 140 K, J_c = 18 K and D = 2.9 K were used in the simulations, where J_{ab} and J_c are the strengths of the intralayer and interlayer Heisenberg exchange, respectively, while D is the strength of interlayer DMI. A value for the easy-plane anisotropy of K = 2.1 K was used. The system size was 32 × 512 × 32 cells (5.75 × 12.10 × 5.75 Å^3 per cell) and periodic boundary conditions were applied in the specimen plane to model the thin nanoplate studied experimentally. In order to simulate changes in periodic CHM order as a function of temperature, the system was annealed from a high

temperature (T = 1000 K) to each target temperature. 500 000 MC steps were performed before calculating the spin configuration at each temperature. The average spin configuration was calculated in real space using 5000 configurations separated by 20 MC steps. The final M_S-T curve in Figure 3(c) (blue line) shows a good match to the experimental results, suggesting that the magnetic behavior of a $CrNb_3S_6$ nanoplate can be described using a three-dimensional classical Heisenberg spin model even in the presence of a reduced dimension in the thickness direction. This robustness to confinement effects can be attributed to the uniform three-dimensional magnetic structure of CHM order in $CrNb_3S_6$, which originates from monoaxial DMI, strong easy-plane anisotropy and strong in-plane exchange interactions.

The period L of CHM order in the nanoplate was then analyzed as a function of temperature. Figure 4(a) shows the period L measured using off-axis EH, LTEM and MC methods. It takes a value of approximately 48 nm over the entire range of investigated temperatures. The similar experimental results are reproduced for another sample in Figure S5 in the Supplemental Material [19]. As a result of the small field of view of off-axis EH measurements, the error in the values of L measured using this technique is relatively large. In order to reduce the error, the nanoplate was also investigated using Fresnel defocus images in LTEM. Representative LTEM images are shown in Figure S6 in the Supplemental Material [19]. A consistent value of $L \sim 48$ nm was measured from the LTEM images across the entire investigated temperature range, in agreement with the off-axis EH results, as well as with previous neutron diffraction results [7,8] and with three-dimensional mean field theory [9,15,23]. In contrast, in previous experimental studies an abnormal decrease in period was reported in a thin $CrNb_3S_6$ lamella over a similar temperature range [15] and was explained using two-dimensional melting theory [24,25]. We believe that the specimen thickness had affected this previous report of the anomalous temperature behavior of the period L if the abnormal behavior was common in $CrNb_3S_6$ thin nanoplate. Therefore, we also studied a wedge-shaped nanostripe with a continuously varying thickness of between 70 and 140 nm to investigate the thickness dependence of the period L. The temperature dependence of CHM order shows the same behavior as that in the nanoplate, as shown in Figure S7 in the Supplemental Material [19]. Measurements of the period L in the wedge-shaped nanostripe are plotted in Figure 4(b) as a function of specimen thickness for different temperatures. The period again shows almost no change with thickness down to 70 nm. The results demonstrate the robustness of the period of CHM order in $CrNb_3S_6$ nanostructures, which is found to be independent of temperature over the investigated range of specimen thickness.

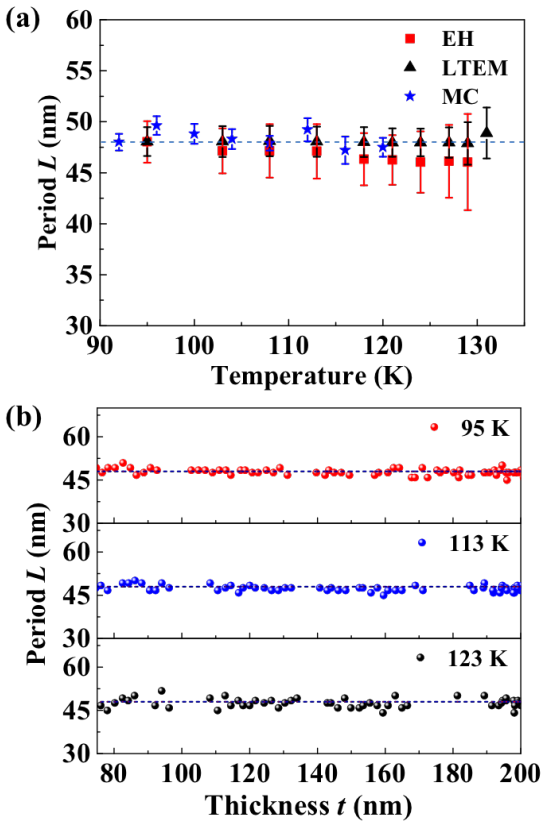

Figure 4. Temperature and thickness dependence of the period of chiral helimagnetic order in $CrNb_3S_6$ nanostructures. (a) Period L of CHM order in a nanoplate that has a fixed thickness of 100 nm measured using off-axis EH (red squares) and Lorentz TEM (black triangles) below the Curie temperature. The period derived from Monte Carlo simulations is marked with blue stars. The dotted line marks a value of 48 nm. (b) Period L of CHM order in a nanostripe that has a continuously varying thickness of between 70 and 240 nm, measured using LTEM and plotted as a function of specimen thickness for different temperatures.

The MC-simulated period of CHM order remains constant over a wide temperature range below the Curie temperature, in agreement with experimental results and three-dimensional mean field theory [9,15,23]. The value of the period L of the CHM order can be expressed in the form $L = 2\pi/\arctan(D/J_c)c_0$, where c_0 is the lattice parameter along the helical axis. The uniformity of the period with temperature suggests that the strength of the two interactions is constant with temperature. This behavior is anticipated because the Heisenberg ferromagnetic exchange and DMI originate from the same exchange tensor. It is safe to assume that D and J are determined by the strong spin-spin coupling and do not change significantly with temperature, even in a free-standing thin nanoplate, resulting in the robust nature of period L for CHM order observed here. Similar situations occur in most skyrmion-hosting materials, including FeGe and MnSi with the B20 structure [4,26]. An exception was reported for B20-type MnGe [27], in which an increased period of skyrmion lattice was reported on approaching the Curie temperature.

The latter behavior can be attributed to the relatively large magnetic anisotropy in this system while absent in $CrNb_3S_6$. Moreover, recent studies have demonstrated that the strength of DMI exhibits a nearly linear correlation with the exchange stiffness [28], resulting in an almost constant period *L*.

In summary, the temperature dependence of the period and saturation magnetization of CHM order in $CrNb_3S_6$ nanostructures has been investigated quantitatively using off-axis electron holography and Monte Carlo calculations. Real space measurements of projected in-plane magnetization provide quantitative information about sinusoidal modulations of CHM order in $CrNb_3S_6$ on the nm scale. The saturated magnetization is measured as a function of temperature and the Curie temperature is determined to be 130 K in a $CrNb_3S_6$ nanoplate, in agreement with results obtained from a bulk crystal and with a classical Heisenberg spin model. The period is found to be independent of temperature and specimen thickness in $CrNb_3S_6$ nanostructures, reproduced in MC simulations and consistent with a three-dimensional classical spin model as well. The present results suggest the robustness and stability of the magnetic characters of CHM order in $CrNb_3S_6$ nanostructures with dimensional confinement, which are important for potential uses of this system in spintronic nanodevices.

ACKNOWLEDGMENTS

This work was also supported by the National Key R&D Program of China, Grant No. 2017YFA0303201; the Key Research Program of Frontier Sciences, CAS, Grant No. QYZDB-SSW-SLH009; the Key Research Program of the Chinese Academy of Sciences, KJZD-SW-M01; the National Natural Science Foundation of China (Grant No. 61801210, 91833302) and the Natural Science Foundation of Jiangsu Province (Grant No. BK20180686). This project has received funding from the European Research Council (ERC) under the European Union's Horizon 2020 research and innovation programme (Grant No. 856538, project “3D MAGiC”). Z. Liu acknowledges the Singapore Ministry of Education under the grant MOE Tier 2 MOE2017-T2-2-136 and MOE Tier 3 MOE2018-T3-1-002.

REFERENCES

[1] N. Kanazawa, S. Seki, and Y. Tokura, Advanced Materials **29**, 1603227 (2017).

[2] S. Seki, X. Z. Yu, S. Ishiwata, and Y. Tokura, Science **336**, 198 (2012).

[3] X. Z. Yu, Y. Onose, N. Kanazawa, J. H. Park, J. H. Han, Y. Matsui, N. Nagaosa, and Y. Tokura, Nature **465**, 901 (2010).

[4] S. Mühlbauer, B. Binz, F. Jonietz, C. Pfleiderer, A. Rosch, A. Neubauer, R. Georgii, and P. Böni, Science **323**, 915 (2009).

[5] F. Zheng, F. N. Rybakov, A. B. Borisov, D. Song, S. Wang, Z.-A. Li, H. Du, N. S. Kiselev, J. Caron, A. Kovács, M. Tian, Y. Zhang, S. Blügel, and R. E. Dunin-Borkowski, Nature Nanotech **13**, 451 (2018).

[6] Y. Togawa, T. Koyama, K. Takayanagi, S. Mori, Y. Kousaka, J. Akimitsu, S. Nishihara, K. Inoue, A. S. Ovchinnikov, and J. Kishine, Physical Review Letters **108**, 107202 (2012).

[7] T. Moriya and T. Miyadai, Solid State Communications **42**, 209 (1982).

[8] T. Miyadai, K. Kikuchi, H. Kondo, S. Sakka, M. Arai, and Y. Ishikawa, J. Phys. Soc. Jpn. **52**, 1394 (1983).

[9] Y. Togawa, Y. Kousaka, K. Inoue, and J. Kishine, J. Phys. Soc. Jpn. **85**, 112001 (2016).

[10] Y. Togawa, Microscopy **62**, S75 (2013).

[11] Y. Togawa, Y. Kousaka, S. Nishihara, K. Inoue, J. Akimitsu, A. S. Ovchinnikov, and J. Kishine, Phys. Rev. Lett. **111**, 197204 (2013).

[12] R. Aoki, Y. Kousaka, and Y. Togawa, Phys. Rev. Lett. **122**, 057206 (2019).

[13] Y. Togawa, T. Koyama, Y. Nishimori, Y. Matsumoto, S. McVitie, D. McGrouther, R. L. Stamps, Y. Kousaka, J. Akimitsu, S. Nishihara, K. Inoue, I. G. Bostrem, Vl. E. Sinitsyn, A. S. Ovchinnikov, and J. Kishine, Phys. Rev. B **92**, 220412(R) (2015).

[14] J.I. Kishine, I. G. Bostrem, A. S. Ovchinnikov, and Vl. E. Sinitsyn, Phys. Rev. B **89**, 014419 (2014).

[15] Y. Togawa, J. Kishine, P. A. Nosov, T. Koyama, G. W. Paterson, S. McVitie, Y. Kousaka, J. Akimitsu, M. Ogata, and A. S. Ovchinnikov, Phys. Rev. Lett. **122**, 017204 (2019).

[16] J.I. Yonemura, Y. Shimamoto, T. Kida, D. Yoshizawa, Y. Kousaka, S. Nishihara, F. J. T. Goncalves, J. Akimitsu, K. Inoue, M. Hagiwara, and Y. Togawa, Phys. Rev. B **96**, 184423 (2017).

[17] G. W. Paterson, T. Koyama, M. Shinozaki, Y. Masaki, F. J. T. Goncalves, Y. Shimamoto, T. Sogo, M. Nord, Y. Kousaka, Y. Kato, S. McVitie, and Y. Togawa, Phys. Rev. B **99**, 224429 (2019).

[18] P. A. Midgley and R. E. Dunin-Borkowski, Nature Materials **8**, 271 (2009).

[19] See Supplemental Material for detailed descriptions of the schematics of $CrNb_3S_6$ nanostructures, sequence of steps to retrieve magnetic phase using off-axis electron holography, real space distributions of the *x* component of projected in-plane magnetization reconstructed using a model-based iterative algorithm, magnetization curve of the bulk $CrNb_3S_6$ crystal as a function of temperature, temperature and thickness dependence of period for two $CrNb_3S_6$ nanoplates and a wedge-shaped nanostripe of $CrNb_3S_6$ measured using the Lorentz Fresnel imaging mode, respectively.

[20] S. L. Y. Chang, C. Dwyer, J. Barthel, C. B. Boothroyd, and R. E. Dunin-Borkowski, Ultramicroscopy **161**, 90 (2016).

[21] E. Völkl, L. F. Allard, and B. Frost, Journal of Microscopy **180**, 39 (1995).

[22] J. Caron, Model-based reconstruction of magnetisation distributions in nanostructures from electron optical phase images, 2018.

[23] M. Shinozaki, S. Hoshino, Y. Masaki, J. Kishine, and Y. Kato, J. Phys. Soc. Jpn. **85**, 074710 (2016).

[24] B. I. Halperin and D. R. Nelson, Phys. Rev. Lett. **41**, 121 (1978).

[25] V. L. Pokrovskii and A. L. Talanov, 15 (1980).

[26] X. Z. Yu, Y. Onose, N. Kanazawa, J. H. Park, J. H. Han, Y. Matsui, N. Nagaosa, and Y. Tokura, Nature **465**, 901 (2010).

[27] T. Tanigaki, K. Shibata, N. Kanazawa, X. Yu, Y. Onose, H. S. Park, D. Shindo, and Y. Tokura, Nano Lett. **15**, 5438 (2015).

[28] Y. Zhou, R. Mansell, S. Valencia, F. Kronast, and S. van Dijken, Phys. Rev. B **101**, 054433 (2020).